Novel Tone Reservation Method for DFT-s-OFDM

Selahattin Gökceli, Ismael Peruga, Esa Tiirola, Kari Pajukoski, Taneli Riihonen, *Member, IEEE*, and Mikko Valkama, *Senior Member, IEEE*

***Abstract*—In this letter, a novel guard-tone reservation (GTR) method is proposed to reduce the peak-to-average power ratio (PAPR) of discrete Fourier transform-spread-orthogonal frequency-division multiplexing (DFT-s-OFDM) waveform. Unlike existing PAPR reduction methods, the proposed GTR operates directly in the data symbol domain, estimating the peaks through the relations between the data symbols, while the corresponding peak-cancellation signal (PCS) is efficiently embedded into the waveform processing. Furthermore, the PCS is generated by exploiting only the guard-band tones, leaving thus the inband data tones undistorted. The performance of the method is evaluated in 5G New Radio (NR) uplink context including also realistic measured power amplifier (PA) characteristics. The obtained results show that significant PAPR reduction and corresponding PA output power gains can be obtained while the computational complexity is shown to be low.**

***Index Terms*—5G new radio, coverage, DFT-s-OFDM, guard-tone, PAPR, power amplifier, power efficiency, tone reservation.**

I. Introduction

THE BASELINE physical-layer waveform of 5G NR [1], [2] is cyclic-prefix (CP) orthogonal frequency-division multiplexing (OFDM), while discrete Fourier transform-spread-OFDM (DFT-s-OFDM) is also supported in uplink (UL) [1], [2], as it is known to have lower peak-to-average power ratio (PAPR). However, with high modulation orders, the PAPR advantages of DFT-s-OFDM, compared to plain OFDM, start to diminish. Additionally, in millimeter-wave networks, or at the so-called frequency range 2 (FR2) [1], [2], efficient PAPR reduction methods are very important for improved power-efficiency and network coverage.

In this letter, tone reservation (TR) is considered as the baseline PAPR reduction approach due to its suitability to the studied problem [3]. The TR is a well-known method with various further detailed variants being available in the literature. However, most of the solutions involve iterative processing and thus come with substantial computational complexity and power consumption, making their application in mobile terminal transmitters challenging. To this end, in [4], a time-domain kernel building on TR tones is used to create the peak-cancellation signal (PCS). This method can cancel one peak in one iteration and since multiple peaks are likely to occur, the method is applied iteratively. Similarly, in [5], a scaling factor that changes the amplitude and phase values of the kernel samples of [4] is computed for the generation of each PCS. This way, multiple peaks can be cancelled in each iteration, but the complexity also increases with respect to [4]. The common problem of both methods is the complexity as operations such as circular shifting, and changing both phase and amplitude of the kernel are required for PCS creation. Additionally, the use of inband tones reduces spectral efficiency.

Besides TR, few other works have specifically addressed the PAPR reduction of DFT-s-OFDM. In [6], the phases of the particular modulated symbols that cause the peaks of the output signal, are modified such that the PAPR is reduced. However, this increases also the link bit error rate (BER). Similar approach is also considered in [7] but different from [6], the BER increase is more controlled. In both studies, it is discovered that consecutive symbols on the outer constellation points and with opposite phases have the highest contribution to the resulting time-domain peaks. This observation is considered as one of the building blocks of this letter, however, it will also be shown that there are additional symbols with considerable impact on peaks, forming further basis for the proposed method.

In this letter, a novel guard-tone reservation (GTR) method is proposed for DFT-s-OFDM PAPR reduction, with specific emphasis on 5G NR uplink. Opposed to existing methods where the full time-domain waveform is commonly created, and iteratively processed through multiple transforms, the proposed method operates directly in the data symbol domain. To this end, a peak detection filter is derived to model how the DFT-s-OFDM processing shapes the input data symbols. Through this, the most notable high-amplitude time-domain peaks can be estimated while also the specific data symbols causing such peaks are detected. Then, to generate the corresponding PCS, applicable guard-band tones are properly configured such that the PAPR of the generated DFT-s-OFDM is reduced. This allows to avoid spectral efficiency losses, while facilitates efficient PCS creation when deployed properly. Additionally, the method does not impact the receiver processing in any way and does not cause any increase in the transmit signal error vector magnitude (EVM) or the fundamental link BER behavior. The performance of the proposed method is evaluated by following the 5G NR guidelines and uplink emission limits, incorporating also a practical measured power amplifier (PA) model. The provided numerical results illustrate the efficiency of the proposed method, while also high-lighting the low computational complexity of the solution.

II. System Model and Proposed Solution

A. DFT-s-OFDM Signal Model

To create DFT-s-OFDM waveform, bits are first mapped to M-QAM or M-PSK data symbols. Within one multicarrier

Manuscript received May 20, 2021; accepted June 28, 2021. Date of publication July 6, 2021; date of current version October 7, 2021. This work was supported in part by the Academy of Finland under Grant 319994, Grant 338224, and Grant 332361; and in part by Nokia Bell Labs. The associate editor coordinating the review of this article and approving it for publication was N. Wu. *(Corresponding author: Mikko Valkama.)*

Selahattin Gökceli, Ismael Peruga, Taneli Riihonen, and Mikko Valkama are with the Department of Electrical Engineering, Tampere University, 33720 Tampere, Finland (e-mail: mikko.valkama@tuni.fi).

Esa Tiirola and Kari Pajukoski are with Nokia Bell Labs, 90620 Oulu, Finland.

Digital Object Identifier 10.1109/LWC.2021.3094887

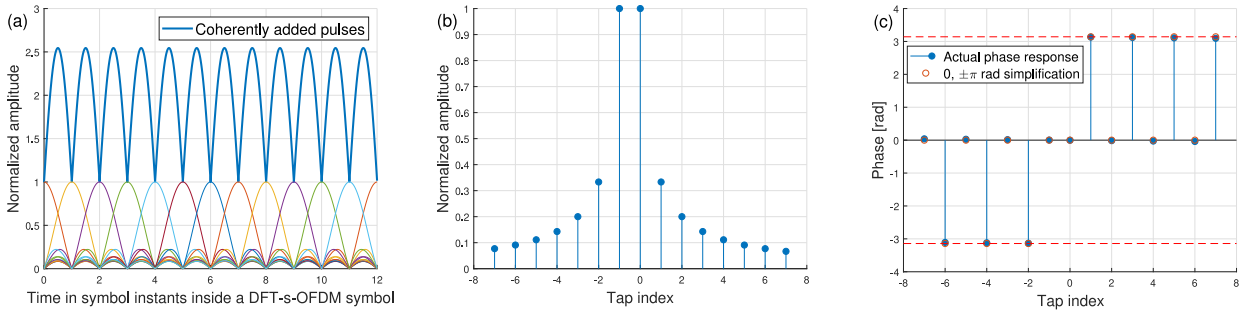

Fig. 1. In (a), the underlying pulses in (3) are illustrated for example numerical values of $N_{\mathrm{DFT}} = 12$ and $N = 1024$. Also the potential of creating peaks to the composite waveform through coherent addition of pulse sidelobes is high-lighted. In (b) and (c), the amplitude and phase behavior of the peak detection filter are shown for $L = 7$, $N_{\mathrm{DFT}} = 612$ and $N = 1024$.

symbol duration, these are denoted by $d[l]$ with $l \in \{0, 1, \ldots, N_{\mathrm{DFT}} - 1\}$. Then, with DFT precoding, the frequency-domain samples are obtained as

$$X[k] = \frac{1}{\sqrt{N_{\mathrm{DFT}}}} \sum_{l=0}^{N_{\mathrm{DFT}}-1} d[l] e^{-j2\pi kl/N_{\mathrm{DFT}}}, \tag{1}$$

where k is the frequency-domain subcarrier index. After zero padding, the oversampled signal is converted to time-domain through IDFT of size N as

$$x[n] = \frac{1}{\sqrt{N}} \sum_{k=-N/2}^{N/2-1} X[k] e^{j2\pi kn/N}, \tag{2}$$

where $n \in \{0, 1, \ldots, N-1\}$ is the index of the corresponding time-domain sample within the considered multicarrier symbol. As shown in [6], and assuming that the active data subcarriers are allocated at the center of the channel, denoted by the set $\mathcal{K}_d = \{-N_{\mathrm{DFT}}/2, \ldots, N_{\mathrm{DFT}}/2 - 1\}$, (2) can also be expressed as

$$\begin{aligned} x[n] &= \frac{1}{\sqrt{N_{\mathrm{DFT}} N}} \sum_{l=0}^{N_{\mathrm{DFT}}-1} d[l] \sum_{k=-N_{\mathrm{DFT}}/2}^{N_{\mathrm{DFT}}/2-1} e^{(j2\pi kn/N - j2\pi kl/N_{\mathrm{DFT}})} \\ &= \frac{1}{\sqrt{N_{\mathrm{DFT}} N}} \sum_{l=0}^{N_{\mathrm{DFT}}-1} d[l] g[n - lN/N_{\mathrm{DFT}}], \end{aligned} \tag{3}$$

where the effective pulse-shaping function $g[\nu]$ reads

$$g[\nu] = e^{-j(\pi\nu/N)} \frac{\sin(\pi N_{\mathrm{DFT}} \nu/N)}{\sin(\pi\nu/N)}. \tag{4}$$

For other contiguous sets of active bins, the expressions in (3) and (4) are similar, except for an extra phase term in (4).

We next shortly address the characteristics of the consecutive pulses in (3), to better understand how the data symbols $d[l]$ are shaped. To this end, by assuming simple example values of $N_{\mathrm{DFT}} = 12$ and $N = 1024$, the amplitude behavior of the consecutive pulses are illustrated in Fig. 1 (a). As can be observed, only a relatively small number of neighboring pulses have considerable impact on a time-domain sample $x[n]$ inbetween the data symbol instants. Additionally, Fig. 1 (a) also illustrates that the potential of the pulse side-lobes to sum up coherently into large peaks in the waveform is highest at the middle of the two symbol instants.

To better quantify this, the normalized squared Euclidean distance (NSED) is measured between a time-domain sample value $x[n]$ and a sum of symbol-weighted pulses over a considered symbol range around $d[l]$. Such NSED metric is explicitly defined as

$$\Psi_{n,l} = \frac{\left| x[n] - \overbrace{\frac{1}{\sqrt{N_{\mathrm{DFT}} N}} \sum_{m=l-L}^{l+L} d[\bar{m}] g[n - \bar{m}N/N_{\mathrm{DFT}}]}^{\text{reconstructed sample}} \right|^2}{|x[n]|^2}, \tag{5}$$

where $\bar{m} = \mathrm{mod}(m, N_{\mathrm{DFT}})$, and thus the reconstructed sample is essentially a result of a cyclic convolution of the considered data symbols and the applicable samples of the involved pulses.

The NSED is next evaluated for 3GPP standard-compliant 5G NR uplink signal with fully-loaded 20 MHz channel and subcarrier spacing (SCS) of 30 kHz, corresponding to $N_{\mathrm{DFT}} = 612$ and $N = 1024$. When considering a large amount of independent data symbol realizations and focusing on the sample values in the middle of the symbol instants, an averaged NSED value of 88% is obtained for $L = 5$. For $L = 10$ and $L = 15$, the corresponding values are 94% and 96%, while increasing L further does not change the value anymore significantly. Thus, a relatively small group of symbols contribute most to the large peaks and other symbols have negligible effect on the peaks due to the low-amplitude coefficients resulting from DFT precoding followed by IDFT. This observation generalizes the claims of [6], where only two symbols are regarded as the main cause of the large peaks.

B. Peak Detection Filter

To reduce the PAPR efficiently, we seek to identify the most problematic symbol groups already before DFT precoding, i.e., in the data symbol domain. To this end, inspired by (5), the peaks can be reconstructed in data symbol domain through circular convolution. Furthermore, Fig. 1 (a) shows that the waveform can potentially present the largest peaks in the middle between two consecutive symbol instants. Thus, any potential peak sample can be reconstructed by sampling the reconstruction expression in (5) in the middle between the lth and $(l+1)$st symbol instants.

To this end, we first define the pulse for the lth symbol (i.e., shifted version of the pulse $g[v]$) as

$$g_l[v] = g[v - lN/N_{\mathrm{DFT}}]. \tag{6}$$

Since the symbol instants of $d[l]$ and $d[l+1]$ are $v = \frac{Nl}{N_{\mathrm{DFT}}}$ and $v = \frac{N(l+1)}{N_{\mathrm{DFT}}}$, the middle point corresponds to $v = \frac{N(l+1/2)}{N_{\mathrm{DFT}}}$. Thus, the reconstructed peak between the symbols $d[l]$ and $d[l+1]$, subject to potential constant scaling,

can be expressed as

$$r_l = \sum_{m=l-L}^{l+L} d[\bar{m}] g_{\bar{m}} \left[\frac{N(l+1/2)}{N_{\mathrm{DFT}}} \right], \tag{7}$$

where $\bar{m} = \mathrm{mod}(m, N_{\mathrm{DFT}})$. The expression in (7) allows us to define a peak reconstruction filter $h[m]$ with $P = 2L + 1$ taps as

$$h[m] = g_{\mathrm{mod}(l-m, N_{\mathrm{DFT}})} \left[\frac{N(l+1/2)}{N_{\mathrm{DFT}}} \right], \tag{8}$$

where $m \in \{-L, -L+1, \ldots, 0, \ldots, L-1, L\}$. This filter is identical for any given data symbol index l, due to circular symmetry of the involved transforms. Additionally, while we are reconstructing the waveform in the middle between the symbol instants l and $(l+1)$, the reconstruction of any other sample can be pursued conceptually similarly, with difference only in the applicable filter coefficients. Finally, the peak reconstruction in (7) can be re-expressed by using the defined peak reconstruction filter as

$$r_l = \sum_{m=l-L}^{l+L} d[\bar{m}] h[l-m]. \tag{9}$$

Example behavior of the peak reconstruction filter amplitudes and phases is shown in Fig. 1 (b) and (c), respectively, for $L = 7$, $N_{\mathrm{DFT}} = 612$ and $N = 1024$ corresponding to 5G NR 20 MHz channel with 30 kHz SCS with active data subcarriers allocated at the center of the channel.

C. Proposed GTR Method

The block-diagram of the overall proposed GTR method is shown in Fig. 2. The main idea is to identify the waveform peaks within an DFT-s-OFDM symbol through the previously described peak detection filtering in data symbol domain, while then properly excite a *set of tones outside the active allocation* to create the peak-cancellation signals. This set of cancellation tones denoted by $\mathcal{K}_g$ is assumed to be located within the guard-band of the NR channel (hence the name guard TR), while properly noting the transmitter emission requirements as elaborated further below. We also note that the network could indicate and allow, through specific signaling, the use of inband tones for peak cancellation that could be shared between multiple frequency multiplexed UEs for controlled loss in cell capacity. However, in this work, we primarily focus on the use of the guard-band tones.

Specifically, the peak reconstruction filtering in (9) is applied in a sliding window manner over the whole block of data symbols $d[l]$, $l \in \{0, 1, \ldots, N_{\mathrm{DFT}} - 1\}$. The corresponding reconstructed amplitude values are then compared to a chosen peak threshold γ, determined based on the target PAPR level, which yields the index set of problematic symbols as

$$\Omega_{\mathrm{PS}}(l) = \begin{cases} l, & \text{if } |r_l| \geq \gamma \\ \emptyset, & \text{otherwise}. \end{cases} \tag{10}$$

As direct side-products, the indices ($\lfloor (l+1/2)N/N_{\mathrm{DFT}} \rceil$) and the phase values ($\angle(r_l)$) of the time-domain peaks are also obtained, where $\lfloor \cdot \rceil$ and $\angle(\cdot)$ represent the rounding operation and phase angle, respectively.

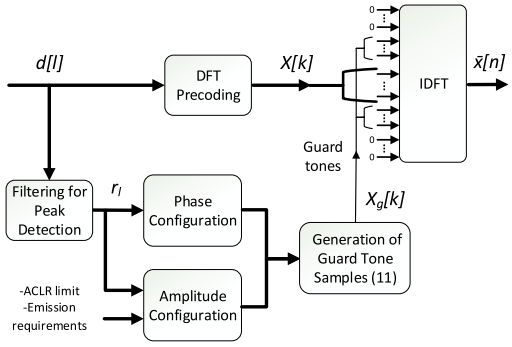

Fig. 2. Block-diagram of the proposed GTR method.

The actual time-domain output sequence at the IDFT output, including also the peak-cancellation tones, can be formally expressed as

$$\bar{x}[n] = \frac{1}{\sqrt{N}} \sum_{k \in \mathcal{K}_d \cup \mathcal{K}_g} \{X[k] + X_g[k]\} e^{j2\pi kn/N}, \tag{11}$$

where $X[k]$, $k \in \mathcal{K}_d$, reads as shown in (1) while $X_g[k]$, $k \in \mathcal{K}_g$ denote the cancellation samples at the considered guard-tones at the IDFT input. Additionally, $X[k] = 0$, $\forall k \notin \mathcal{K}_d$ while $X_g[k] = 0$, $\forall k \notin \mathcal{K}_g$. To define the samples $X_g[k]$ at the cancellation tones, we next express the IDFT of arbitrary $X_g[k]$, $k \in \mathcal{K}_g$, evaluated at the instants where the peaks have been detected, as

$$x_g\left[(l+1/2)\frac{N}{N_{\mathrm{DFT}}}\right] = \sum_{k \in \mathcal{K}_g} X_g[k] e^{j2\pi k \frac{(l+1/2)}{N_{DFT}}}, \; l \in \Omega_{\mathrm{PS}}. \tag{12}$$

Thus, to obtain time-domain cancellation samples that have opposite phases to those of the detected peaks, the cancellation samples at the guard-tones are generated as

$$X_g[k] = \sum_{l \in \Omega_{\mathrm{PS}}} A_g(l) e^{\left\{-j\left(\angle r_l + \frac{2\pi k(l+1/2)}{N_{\mathrm{DFT}}}\right)\right\}}, \; \forall k \in \mathcal{K}_g, \tag{13}$$

where r_l is the output of the peak detection filter in (9). Moreover, $A_g(l)$ in (13) refers to the amplitude value configured for cancelling the peak that is caused by the symbol $l \in \Omega_{\mathrm{PS}}$. This can be computed by calculating the difference between the reconstructed peak amplitude and the amplitude threshold that corresponds to the target PAPR level while further dividing it by the number of guard-band tones N_g. If the resulting amplitude of $X_g[k]$ exceeds the level allowed by the out-of-band (OOB) emission limits, we assume that the amplitude is normalized to this level, such that the emission requirements are not violated. We note that the power limit on the cancellation tones at guard-band limits also the PAPR reduction capability; however, the numerical results in Section III evidence still good performance.

D. Low-Complexity Implementation

As illustrated already in Fig. 1 (b) and (c), the structure of the peak detection filter allows for efficient implementations. Specifically, as the phases of the tap coefficients are essentially either zero or $\pm\pi$, the taps are real-valued. Additionally, there is clear symmetry around the two center taps, which further decreases the implementation complexity, compared to filtering with arbitrary complex-valued taps.

To further reduce the complexity, the peak detection filtering can be pursued in multiple cascaded stages. Specifically, since the central taps have the highest impact on peaks, a short filter of say $P = 3$ taps can be first deployed to identify an initial index set of the problematic symbols, denoted as $\Omega_{\mathrm{PS}}^{(1)}$. This initial set of symbols can then be further processed with longer filters, to better and more accurately identify the final index set Ω_{PS}. The complexity in these further processing stages is already clearly lower, despite relatively longer filters, as the set of symbols has already been substantially reduced.

As a concrete example, by doing the filtering in three stages with $P = 3$ (first stage, $\Omega_{\mathrm{PS}}^{(1)}$), $P = 4$ (second stage, $\Omega_{\mathrm{PS}}^{(2)}$), and $P = 15$ (third stage, Ω_{PS}), the overall complexity of GTR including PCS creation is $22|\Omega_{\mathrm{PS}}^{(2)}| + 2N_g|\Omega_{\mathrm{PS}}|$ real multiplications and $4N_{\mathrm{DFT}} + 2|\Omega_{\mathrm{PS}}^{(1)}| + 22|\Omega_{\mathrm{PS}}^{(2)}| + 4N_g|\Omega_{\mathrm{PS}}|$ real additions per DFT-s-OFDM symbol containing N_{DFT} data symbols. While in general the length of the deployed peak detection filter is a trade-off between processing complexity and peak detection performance, we use the above configuration in the following numerical results, and show that very efficient PAPR reduction can be obtained with very low complexity compared to the existing reference methods.

III. Numerical Results and Analysis

A. Scenarios, Assumptions and Metrics

The performance of the proposed method is next evaluated numerically and compared against existing reference methods [4], [5] and the well-known iterative clipping and filtering (ICF) approach [8]. As the main performance metrics, PAPR distribution, ACLR, and maximum PA output power are considered. Also the EVM is considered in the context of maximum PA output power evaluation, but excluded otherwise since the proposed method does not cause any EVM or BER degradation to the digital waveform. The ACLR is evaluated by following the 5G NR guidelines, while also the corresponding UL spectrum emission mask (SEM) [9, Sec. 6] assessment is included in the results. To improve the baseline waveform spectrum confinement, weighted overlap-and-add processing with window length of 35% of the CP length, is applied. In GTR, the PD filter with $P = 15$ is utilized in the third stage.

In the evaluations, an example target PAPR level of 5 dB is considered when calculating the symbol-domain peak detection filter threshold γ, while then the actual realized PAPR is measured through the sample-wise PAPR distribution over long signal realizations comprising complete radio-frames of 10 ms. Moreover, three different 5G NR channel bandwidth cases of 5 MHz, 10 MHz and 20 MHz are considered with 64-QAM modulation. For each case, applicable uplink SCS values within 15 kHz, 30 kHz and 60 kHz are adopted following [9], while full channel allocations are considered for simplicity. Additionally, as in [10], oversampling with a factor of $N_{\mathrm{OS}} = 4$ is applied to achieve accurate representation of the PAPR which means four times larger IDFT sizes (values of N) compared to baseline IDFT sizes ($N_{\mathrm{OS}} = 1$). For reference, however, results with $N_{\mathrm{OS}} = 1$ are also evaluated. Finally, all IDFT bins belonging to the guard-band inside the channel bandwidth are always utilized for PCS creation, except for the two bins at both channel edges, such that meeting the SEM mask is feasible.

B. Results and Discussion

As the first example, the PAPR distributions for 20 MHz channel bandwidth and SCS of 30 kHz ($N_{\mathrm{DFT}} = 612$, $N_{\mathrm{OS}} = 4$ and $N = 4096$) are shown in Fig. 3 (a), without and with the proposed GTR processing, while the corresponding distribution for CP-OFDM is shown for reference. At the CCDF level of 0.01%, CP-OFDM has a very high PAPR of 9.6 dB, while the corresponding number of DFT-s-OFDM is 7.7 dB. Then, the proposed GTR is able to reduce the PAPR further, down to approximately 6.4 dB with the deployed value of $P = 15$ and the amount of the available guard-tones. Additionally, the figure also shows that similar performance is obtained in all considered channel bandwidth and SCS cases.

Next, the power spectral density (PSD) of the PAPR reduced digital signal is shown in Fig. 3 (b). While the guard-band tones are now containing the cancellation samples, the figure illustrates that the SEM mask is still properly fulfilled. Additionally, the ACLR of the digital waveform is still excellent, being approximately 74 dB in this numerical example. Hence, there is still a large gap to the 5G NR uplink ACLR of 30 dB corresponding to the power class 3 UEs [9].

Furthermore, the GTR method is compared against ICF and the reference methods in [4] and [5]. Both ICF and the TR variants are iterative methods and are here applied in the DFT-s-OFDM context. Specifically, a 20 MHz 5G NR channel is configured with SCS of 60 kHz ($N_{\mathrm{DFT}} = 288$). Due to the assumed power limit for the PAPR reduction tones and the processing differences among the methods, each method is independently parameterized such that similar realized PAPR values can be obtained. Specifically, this yields the target PAPR values of 5 dB for GTR, 6 dB for [4], and 6.4 dB for [5] and the ICF. The corresponding realized PAPR CCDF results for all the four methods are collected and presented in Table I, at two CCDF levels, and including also two different oversampling factors of $N_{\mathrm{OS}} \in \{1, 4\}$, implying $N \in \{512, 2048\}$. As can be observed, the reference methods provide very similar PAPR performance compared to the proposed GTR method. However, the GTR method does not infer any loss in link performance (inband distortion or spectral efficiency loss), while offers also substantially lower processing complexity. This is addressed in further details next.

The computational complexities of the proposed GTR method and the considered reference methods are next assessed and compared. Here, the complexities are evaluated in terms of the needed real multiplications and additions, while the complexity of the plain DFT-s-OFDM without any PAPR reduction is used as reference, considering the same values of N and N_{DFT} as the PAPR reduction methods. As shown in Table I, the GTR method increases the number of real multiplications and additions by 23% and 21% with respect to plain DFT-s-OFDM when $N_{\mathrm{OS}} = 1$. On the other hand, the TR-based reference methods increase the multiplications by 179% and 404%, and the additions by 113% and 128%, respectively.

Furthermore, when $N_{\mathrm{OS}} = 4$ is considered, values of the GTR method drop to 5.6% and 5.5%, respectively. The corresponding increases in multiplications are 44% and 99% for the two TR variants, while for the additions increase by 29% and 32%, respectively. The ICF reference runs four iterations to realize the PAPR target resulting in a large increase in the complexity, as each iteration needs one IDFT/DFT pair.

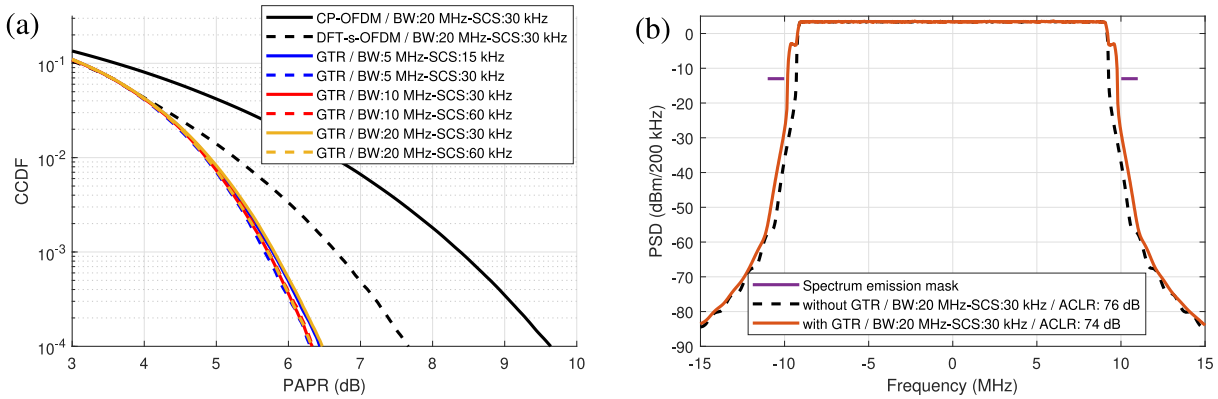

Fig. 3. Example DFT-s-OFDM PAPR distributions without and with the proposed GTR method are shown in (a) covering different 5G NR channel bandwidth and subcarrier spacing configurations. The PAPR target for peak detection is 5 dB. Also the CP-OFDM PAPR behavior is shown for reference. An example PSD behavior of the digital waveform with GTR processing is shown in (b), depicting also the UL SEM up to 1 MHz offset for 200 kHz measurement bandwidth.

TABLE I
PAPR RESULTS WITH CORRESPONDING RELATIVE PROCESSING COMPLEXITIES FOR 20 MHZ 5G NR CHANNEL AND 60 KHZ SCS

Case	GTR		Ref #1 [4]		Ref #2 [5]		ICF	
N_{OS}	1	4	1	4	1	4	1	4
PAPR 0.1%	5.9 dB	5.9 dB	5.9 dB	5.9 dB	5.9 dB	5.9 dB	5.3 dB	5.2 dB
PAPR 0.01%	6.5 dB	6.5 dB	6.5 dB	6.5 dB	6.4 dB	6.4 dB	6.4 dB	6.4 dB
Increase in mult.	23%	5.6%	179%	44%	404%	99%	800%	800%
Increase in add.	21%	5.5%	113%	29%	128%	32%	800%	800%

Overall, the complexity numbers show that the proposed GTR method is computationally very efficient compared to the reference methods, while facilitating high-performance PAPR reduction. The higher complexity of the TR-based reference methods is mainly due to the post-IDFT processing. Specifically, since the length of the time-domain DFT-s-OFDM symbol waveform is quite long, especially for larger IDFT sizes, the amount of additions and multiplications required for the PCS generation impact the complexity of the reference methods significantly. The proposed approach, in turn, operates in the pre-IDFT or data symbol domain, thus allowing for largely reduced complexity. The ICF, in turn, is known to facilitate very good PAPR reduction performance; however, it also poses very substantial processing complexity as seen in Table I. Additionally, it degrades the EVM due to inband clipping noise, which in this example is around 2–3%.

Finally, the maximum transmit power gain available through the GTR method is evaluated by considering all 5G NR Rel-16 uplink emission measurements and the corresponding specifications at FR1 [9] together with a measured terminal PA model. The power contained to the cancellation tones is less than 2% of the total power but is taken properly into account in the assessment. In the different channel bandwidth and SCS cases, the obtained PA output power gains compared to plain DFT-s-OFDM waveform range between 0.7–0.9 dB while still meeting all RF emission limits. With the PA model involved, the maximum transmit power is observed to be ACLR limited. Such increases in the achievable transmit power have a substantial impact on the uplink coverage.

IV. CONCLUSION

In this letter, a novel guard-tone reservation method was proposed for reducing the PAPR of DFT-s-OFDM waveform. Stemming from the waveform modeling, the GTR method estimates the largest peaks and the corresponding data symbol groups directly in the data symbol domain, while guard-tones are then exploited to generate the corresponding peak-cancellation signals to suppress the peaks. Through 5G NR standard compliant numerical results, it was shown that the proposed method allows for efficient PAPR reduction, while being substantially less complex in terms of computations compared to state-of-the-art reference methods. Additionally, the proposed method does not impact the data symbols in any way, which is particularly important for high modulation orders, while still allowing for efficient PAPR reduction.

REFERENCES

[1] E. Dahlman, S. Parkvall, and J. Sköld, *5G NR: The Next Generation Wireless Access Technology*. New York, NY, USA: Academic, 2018.
[2] *New Radio (NR); Overall Description; Stage-2, V16.0.0*, 3GPP Standard TS 38.300, Dec. 2019.
[3] J. Hou, J. Ge, and F. Gong, "Tone reservation technique based on peak-windowing residual noise for PAPR reduction in OFDM systems," *IEEE Trans. Veh. Technol.*, vol. 64, no. 11, pp. 5373–5378, Nov. 2015.
[4] J. Tellado, *Multicarrier Modulation With Low PAR: Applications to DSL and Wireless*. New York, NY, USA: Springer, 2000. [Online]. Available: https://www.springer.com/gp/book/9780792379881
[5] P. Yu and S. Jin, "A low complexity tone reservation scheme based on time-domain kernel matrix for PAPR reduction in OFDM systems," *IEEE Trans. Broadcast.*, vol. 61, no. 4, pp. 710–716, Dec. 2015.
[6] J. Ji, G. Ren, and H. Zhang, "PAPR reduction in coded SC-FDMA systems via introducing few bit errors," *IEEE Commun. Lett.*, vol. 18, no. 7, pp. 1258–1261, Jul. 2014.
[7] K. Wu, G. Ren, and M. Yu, "PAPR reduction of SC-FDMA signals using optimized additive pre-distortion," *IEEE Commun. Lett.*, vol. 19, no. 8, pp. 1446–1449, Aug. 2015.
[8] J. Armstrong, "Peak-to-average power reduction for OFDM by repeated clipping and frequency domain filtering," *Electron. Lett.*, vol. 38, no. 5, pp. 246–247, Feb. 2002.
[9] *NR; User Equipment (UE) Radio Transmission and Reception; Part 1: Range 1 Standalone*, 3GPP Standard TS 38.101-1, Jun. 2019.
[10] H. Ochiai and H. Imai, "Performance analysis of deliberately clipped OFDM signals," *IEEE Trans. Commun.*, vol. 50, no. 1, pp. 89–101, Jan. 2002.